Fuel 421 (2026) 139123

Contents lists available at ScienceDirect

Fuel

journal homepage: www.elsevier.com/locate/jfue

Full length article

Autoignition and flame dynamics of a methanol droplet in hydrogen-enriched air

Zhiwu Jiang [a, b], Shangpeng Li [c,*], Zheng Chen [a], Huangwei Zhang [c,*]

[a] Department of Mechanics and Engineering Science, College of Engineering, Peking University, Beijing, 100871, China
[b] Advanced Manufacturing Materials Centre, National University of Singapore (Chongqing) Research Institute, Chongqing, 401120, China
[c] Department of Mechanical Engineering, National University of Singapore, 117576, Singapore

HIGHLIGHTS

- Interface-resolved VOF simulations of methanol droplet autoignition with hydrogen.
- Ambient temperature and hydrogen variation reveal five distinct ignition regimes.
- Hydrogen enrichment produces two-stage ignition with bi-directional premixed flames.
- Hydrogen decreases ignition delays with diminishing gains at higher concentrations.

ARTICLE INFO

Keywords:
Methanol droplet
Hydrogen enrichment
Autoignition
Two-stage ignition
Flame dynamics
VOF simulation

ABSTRACT

Methanol is a promising low-carbon fuel and liquid hydrogen carrier for future decarbonized energy systems, but its relatively low reactivity limits ignition and flame stabilization in practical devices. Enriching the oxidizer with hydrogen has been proposed to compensate for these limitations; however, the micro-scale interactions between an evaporating methanol droplet and hydrogen-enriched air remain poorly understood. This study presents an interface-resolved numerical investigation of the autoignition and early flame dynamics of an isolated methanol droplet suspended in hot, hydrogen-enriched air under zero-gravity conditions. A volume-of-fluid framework, coupled with well-validated skeletal gas-phase chemical kinetics and multicomponent transport, is employed to quantify the effects of ambient temperature and hydrogen mass fraction on ignition delays, ignition locations, and subsequent flame evolution. By varying the ambient temperature from 800 to 950 K and the ambient hydrogen mass fraction from 0 to 0.01, five ignition regimes are identified: non-ignition, low-hydrogen single-stage ignition, medium-hydrogen two-stage ignition, high-hydrogen two-stage ignition, and high-temperature global hydrogen ignition. A key outcome is the emergence of two-stage ignition at intermediate and high hydrogen levels, in which remote autoignition of the hydrogen-air mixture produces a pair of bi-directional premixed flames. Hydrogen enrichment systematically reduces both first- and second-stage ignition delays, with diminishing returns at higher hydrogen levels, while the first-stage ignition location exhibits a non-monotonic dependence on hydrogen concentration at lower ambient temperatures. These results clarify the fundamental mechanisms governing dual-fuel droplet autoignition and flame topology in hydrogen-enriched environments and provide guidance for the design of advanced combustion systems employing methanol-hydrogen blends.

1. Introduction

The global transition toward low-carbon energy systems has intensified interest in clean fuels and effective hydrogen carriers capable of partially or fully replacing conventional hydrocarbons [1,2]. Among various candidates, methanol stands out due to its simple molecular structure, relatively high hydrogen-to-carbon ratio, low soot propensity, and the possibility of renewable production from biomass or CO_2 hydrogenation [3–5]. These features make methanol attractive for low-emission engines, industrial burners, and as a practical liquid vector within emerging hydrogen economies [1].

Despite these advantages, methanol exhibits relatively low laminar burning velocities and moderate chemical reactivity compared with hydrogen-rich fuels. To alleviate these limitations, blending methanol

* Corresponding authors.
Email addresses: li-sp@nus.edu.sg (S. Li), huangwei.zhang@nus.edu.sg (H. Zhang).

https://doi.org/10.1016/j.fuel.2026.139123
Received 23 December 2025; Received in revised form 5 March 2026; Accepted 10 March 2026
Available online 13 March 2026

with hydrogen has been widely proposed and examined in both premixed flames and engine configurations [6–8]. Hydrogen enrichment increases flame speed, broadens flammability limits, and elevates the pool of reactive radicals, thereby accelerating ignition chemistry and flame propagation [7,9]. Laminar flame studies have confirmed substantial increases in flame speed with hydrogen addition [7], while engine experiments have reported improved combustion efficiency, extended lean limits, and reduced pollutant emissions [6,8]. Collectively, these studies demonstrate that modest hydrogen supplementation can effectively compensate for several intrinsic limitations of methanol combustion.

In practical systems such as spark-ignition engines, gas turbines, and industrial furnaces, liquid fuels are typically injected as sprays. At this scale, droplet evaporation, mixing, autoignition, and burning govern the global flame structure, pollutant formation, and stability characteristics [10–13]. Isolated single-droplet configurations therefore remain indispensable canonical problems for deconstructing these complex interactions [12,14]. Over several decades, numerous experimental and numerical studies have demonstrated that droplet ignition and combustion are controlled by the tightly coupled interplay among liquid-phase vaporization, interfacial heat and mass transfer, and detailed gas-phase kinetics [15–20].

While there is a rich literature on single-fuel droplet autoignition and on gaseous methanol-hydrogen flames, the fundamental autoignition and flame dynamics of a liquid methanol droplet in hydrogen-enriched air remain poorly understood. Most previous droplet studies have focused on pure hydrocarbons or alcohols in hydrogen-free oxidizers, quantifying ignition delays, analyzing the effects of convection and ambient temperature, and identifying transitions between kinetics-controlled and diffusion-controlled burning [15,16,19–21]. Under hydrogen-enriched conditions, however, the influence of hydrogen addition on the coupled evaporation and ignition processes of a methanol droplet is still unknown, as are the potential new ignition modes that may arise from hydrogen's active participation in both the pre-ignition stage and subsequent flame propagation.

To address this knowledge gap, the present study undertakes a high-fidelity, interface-resolved numerical investigation of the autoignition of an isolated methanol droplet in quiescent, high-temperature, hydrogen-enriched air. A volume-of-fluid (VOF) framework coupled with detailed chemical kinetics and multicomponent transport is employed to systematically assess the effects of ambient temperature and hydrogen concentration on ignition delay, ignition modes, and flame evolution. The insights obtained provide a fundamental basis for understanding dual-fuel droplet ignition and offer practical guidance for the design of advanced combustion strategies in methanol-hydrogen systems.

2. Physical model and numerical methodology

2.1. Problem configuration

We investigate the autoignition and combustion of an isolated, spherical methanol droplet suspended in quiescent, hydrogen-enriched air under zero-gravity conditions. While practical engines involve complex turbulent spray dynamics, this canonical setup eliminates the confounding effects of buoyancy, convection, and droplet-droplet interactions. It therefore allows the intrinsic coupling between methanol evaporation and hydrogen-assisted ignition to be isolated, providing a fundamental baseline for understanding more complex dual-fuel combustion systems.

The initial droplet diameter and temperature are set to $d_0 = 1$ mm and $T_{d,0} = 300$ K, respectively. The surrounding gas is maintained at a constant pressure of $p = 1$ atm and initialized at a uniform temperature $T_{g,\infty}$. Hydrogen enrichment of the ambient air is specified by the initial hydrogen mass fraction $Y_{H_2,\infty}$, while the oxygen concentration is fixed at the standard air value $Y_{O_2,\infty} = 0.23$.

A parametric study is conducted for ambient temperatures $T_{g,\infty}$ = 800–950 K and hydrogen mass fractions $Y_{H_2,\infty}$ = 0–0.01, enabling systematic examination of the combined thermal and compositional effects on droplet autoignition behavior. For each condition, the system is initialized with quiescent gas and liquid. The simulations evolve from the purely evaporative stage through pre-ignition chemistry and, where applicable, autoignition and subsequent flame propagation.

It should be noted that the selected initial droplet diameter is widely used in microgravity droplet-combustion studies [12,14], as it provides a clear separation between evaporation and ignition timescales and facilitates detailed examination of ignition transients and flame development. The relatively large droplet size results in ignition and burning processes that occur over longer timescales than those typically encountered in practical spray combustion systems. In addition, some simulated ambient hydrogen concentrations may exceed the flammability limit of premixed hydrogen-air mixtures at elevated temperatures. Nevertheless, these conditions are considered here to explore the fundamental physicochemical coupling between methanol evaporation and hydrogen-assisted ignition, which may also arise locally and transiently in practical combustion environments.

2.2. Mathematical formulation

The gas-liquid system is modeled using a one-fluid Eulerian framework. A marker function α represents the local liquid volume fraction, with $\alpha = 1$ in the pure liquid, $\alpha = 0$ in the pure gas, and $0 < \alpha < 1$ in the interfacial region. The gas-liquid interface is captured using the VOF method. The governing equations for conservation of marker function, mass, momentum, sensible enthalpy, and gas-phase species are solved for the mixture fields following Refs. [22,23].

Mixture fields such as density ρ, velocity $\mathbf{V}$, pressure p, and sensible enthalpy h^s satisfy the usual conservation equations with appropriate source terms due to phase change and chemical reactions. The mixture transport properties (viscosity, thermal conductivity, and specific heat) are evaluated as volume-fraction-weighted averages of the gas- and liquid-phase properties. Gas-phase species mass fractions Y_i evolve according to convection-diffusion-reaction equations, with diffusive fluxes computed using a mixture-averaged formulation.

The local mass evaporation flux at the interface is not prescribed via empirical correlations. Instead, it is obtained directly from the interfacial mass balance [22,23], ensuring a consistent coupling between phase change and gas-phase transport and chemistry.

To account for radiative energy exchange during the pre-ignition phase, an additional source term is included in the energy equation. An optically thin radiation model is employed, considering H_2O, CO, CO_2, and CH_4 as the dominant radiating species [22].

Water absorption into the liquid phase is known to play an important role for hygroscopic fuels such as methanol during long-duration microgravity combustion, particularly in the quasi-steady burning stage [22–26]. The present study focuses on pre-ignition and early post-ignition dynamics, for which both the total amount of absorbed water and its impact on the energy balance remain limited. To isolate the effects of hydrogen enrichment on the autoignition chemistry and flame development, water absorption into the droplet is therefore neglected. This simplification is acknowledged and should be revisited in future work addressing long-term burning, extinction, or droplet boiling.

2.3. Thermophysical properties and chemical kinetics

Gas-phase thermodynamic and transport properties are evaluated using the mixture-averaged formulation implemented in the *Cantera* software suite [27]. Liquid-phase properties of methanol, including density, viscosity, thermal conductivity, specific heat, and enthalpy of vaporization, are obtained from correlations provided in the VDI Heat Atlas [28].

Gas-phase chemical kinetics are modeled using the skeletal mechanism for methanol combustion developed by Fernández-Tarrazo et al. [29], which comprises 18 species and 38 reaction steps. This mechanism has been validated over a broad range of conditions relevant to

the present study and includes hydrogen oxidation pathways and key radical species necessary for describing hydrogen-enriched autoignition.

2.4. Numerical implementation

Simulations are performed using *reactingEvaporatingDropletFoam* [23], an in-house solver developed within the *OpenFOAM* framework and based on *DropletSMOKE++* [30]. Exploiting spherical symmetry, the problem is reduced to a one-dimensional (1D) radial domain extending from the droplet center to $r_{\max} = 200\, r_{d,0}$, which is sufficiently large to mimic droplet ignition and combustion in an infinite environment.

At the outer boundary ($r = r_{\max}$), a zero-gradient condition is imposed for velocity, while pressure, temperature, and species mass fractions are fixed at their ambient values. The computational domain is discretized using a non-uniform mesh, refined near the droplet surface with a minimum spacing of 0.2 μm to resolve the thermal and compositional boundary layers in the near field. Grid spacing is progressively increased toward the far field, where gradients diminish, and the maximum cell size is capped at 20 μm to maintain sufficient resolution of the outward propagating flame front.

An operator-splitting strategy is adopted to couple transport and chemistry. The transport equations are advanced using a global time step below 2 μs to satisfy the Courant-Friedrichs-Lewy (CFL) stability constraint. The CFL number is evaluated using the local maximum flow velocity magnitude, accounting for both Stefan flow and thermal expansion caused by combustion, and is strictly maintained below 0.5 for all cells to ensure numerical stability. Within each global time step, chemical source terms are integrated using a stiff ODE solver from *Cantera* with adaptive sub-stepping to accurately capture the fast time scales associated with autoignition chemistry. Grid and time-step refinement studies confirm that ignition delay times, peak temperatures, and integral metrics are insensitive to further refinement, verifying the accuracy and robustness of the numerical approach.

To maintain computational feasibility, simulations are terminated when the droplet radius decreases to 20% of its initial value ($r_d = 0.2\, r_{d,0}$). At this stage, over 99% of the fuel mass has been consumed. As this study focuses on autoignition and early flame development, this termination criterion does not affect the reported results.

3. Results and discussion

3.1. Global autoignition and combustion characteristics

Fig. 1 summarizes the temporal evolution of key global quantities for methanol droplets at $T_{g,\infty} = 900$ K and $Y_{H_2,\infty} = 0$, 0.001, 0.002, and 0.003. Specifically, Fig. 1(a) shows the evolution of the squared droplet diameter d^2. For all cases, the regression of d^2 is approximately linear both before and after ignition, consistent with the classical d^2-law. The slope of the d^2 curve exhibits a clear kink at the onset of ignition: during the purely evaporative phase, the regression rate is relatively small, whereas following ignition the slope becomes significantly steeper, reflecting the enhanced heat transfer from the surrounding flame to the droplet. At a fixed ambient temperature, increasing $Y_{H_2,\infty}$ systematically advances the kink position and thus reduces the ignition delay. The incremental reduction in delay, however, rapidly diminishes with hydrogen enrichment: the difference between $Y_{H_2,\infty} = 0$ and 0.001 is substantial, whereas further increases from 0.002 to 0.003 lead to only marginal additional shortening. This behavior indicates that modest hydrogen addition is sufficient to activate the dominant chain-branching pathways controlling ignition.

The evolution of the instantaneous droplet evaporation rate, shown in Fig. 1(b), mirrors the d^2 trends. During the pre-ignition phase, the evaporation rate increases gradually as the droplet warms. Immediately after ignition, the evaporation rate exhibits an abrupt jump due to the sudden increase in radiative and conductive heat flux from the newly

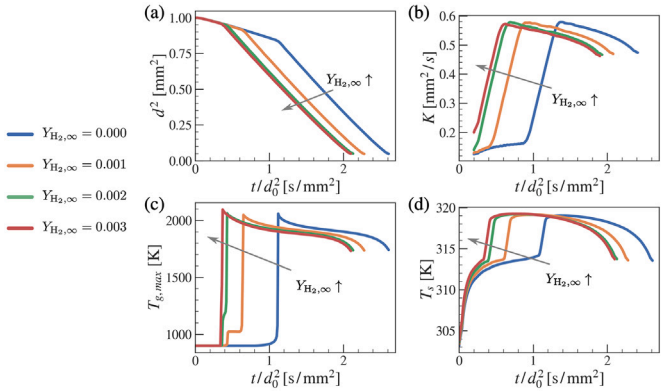

Fig. 1. Temporal evolution of global droplet quantities for different ambient hydrogen mass fractions ($T_{g,\infty} = 900$ K): (a) squared droplet diameter; (b) droplet evaporation rate; (c) maximum gas temperature in the domain; and (d) droplet surface temperature.

formed flame. At later times, as the droplet shrinks and the flame weakens, the evaporation rate gradually declines. The post-ignition evaporation histories for different hydrogen mass fractions nearly collapse onto one another, indicating that, under the moderate hydrogen enrichments considered, the global burning rate of the methanol droplet is governed primarily by interfacial transport rather than by modest variations in flame structure.

Figs. 1(c) and (d) present the maximum gas temperature in the domain, $T_{g,\max}$, and the droplet surface temperature, T_s, respectively. Before ignition, $T_{g,\max}$ remains very close to the ambient value $T_{g,\infty}$ for all hydrogen levels, and the weak pre-ignition chemistry produces negligible heat release. Once ignition occurs, $T_{g,\max}$ exhibits a sharp jump to peak flame temperatures, followed by a gradual decline as the droplet diameter decreases. Because the considered hydrogen mass fractions are relatively small, the peak flame temperatures vary only weakly with $Y_{H_2,\infty}$; hydrogen enrichment primarily shifts the timing of the temperature excursion rather than its magnitude.

The droplet surface temperature T_s exhibits a continuous increase throughout the pre-ignition phase, as shown in Fig. 1(d). Initially, T_s rises rapidly from 300 K due to convective and diffusive heat transfer from the hot ambient gas. As evaporation intensifies, the latent heat of vaporization introduces a competing cooling effect, causing the heating rate to gradually decrease and T_s to approach a quasi-equilibrium value determined by the balance between external heat input and evaporative cooling. This trend is clearly visible in the hydrogen-free case. Hydrogen enrichment does not qualitatively alter the pre-ignition evolution but slightly accelerates the approach to quasi-equilibrium by weakly enhancing pre-ignition reaction rates. At the moment of ignition, the additional heat released in the gas phase leads to a marked jump in T_s, reflecting the sudden intensification of flame-to-droplet heat feedback. During the subsequent diffusion-controlled burning stage, T_s slowly decreases as the droplet radius shrinks and the flame weakens, consistent with the gradual reduction in evaporation rate and $T_{g,\max}$ discussed above.

Fig. 2 presents radius-time (r-t) diagrams of gas temperature and hydrogen mass fraction for two limiting cases at $T_{g,\infty} = 900$ K: hydrogen-free air and relatively strong enriched air with $Y_{H_2,\infty} = 0.01$. In the hydrogen-free case, shown in Figs. 2(a-1,a-2), the gas temperature remains close to $T_{g,\infty}$ until a classical single-stage ignition event occurs in the methanol-air mixture surrounding the droplet. The ignition kernel forms in the vapor-air mixture at a certain distance from the droplet and rapidly evolves into a nearly spherical diffusion flame that envelops the droplet and slowly shrinks inward. The temperature elevation is confined within a region spanning roughly $r \lesssim 20\, r_{d,0}$ during the burning stage. Although the initial ambient gas contains no hydrogen,

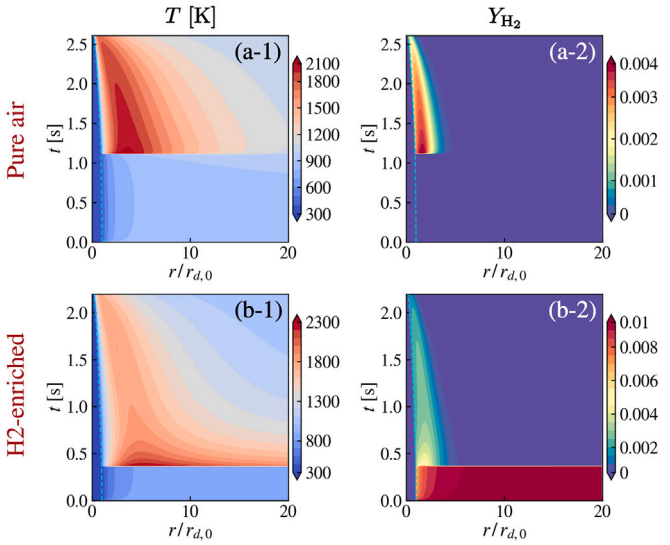

Fig. 2. Radius-time diagrams of gas temperature and hydrogen mass fraction for two limiting oxidizer conditions ($T_{g,\infty}$ = 900 K). Panels (a-1) and (a-2) show, respectively, the gas temperature and H_2 mass fraction in hydrogen-free air ($Y_{H_2,\infty} = 0$). Panels (b-1) and (b-2) show the corresponding fields for hydrogen-enriched air with $Y_{H_2,\infty} = 0.01$. The dashed line denotes the instantaneous droplet interface.

the Y_{H_2} contours in Fig. 2(a-2) reveal the formation of a hydrogen-rich layer between the droplet surface and the flame after ignition, originating from methanol decomposition as an intermediate in the oxidation process. Its presence illustrates the important role of hydrogen-containing radicals, even in nominally hydrogen-free environments, in sustaining droplet flames.

In the hydrogen-enriched case with $Y_{H_2,\infty} = 0.01$, shown in Figs. 2(b-1,b-2), the ignition dynamics are markedly different. The relatively high initial hydrogen content renders the ambient mixture more reactive. Autoignition occurs almost simultaneously in a broad radial region around the droplet, producing a nearly homogeneous temperature rise rather than a localized ignition kernel. This behavior is characteristic of a global, hydrogen-dominated ignition mode. Immediately after this spatially extended ignition event, a high-temperature shell is established that encompasses the droplet. The corresponding Y_{H_2} contours show that hydrogen in a large domain surrounding the droplet is rapidly consumed, leading to a pronounced depletion zone. At later times, as the methanol droplet continues to evaporate and burn, the local hydrogen mass fraction in the domain is dominated by hydrogen produced as an intermediate from methanol oxidation, rather than by the initial ambient hydrogen. Consequently, the flame structure and local hydrogen levels during the quasi-steady diffusion-controlled burning stage become very similar to those in hydrogen-free air.

3.2. Ignition regimes and flame topologies

By systematically varying $Y_{H_2,\infty}$ from 0 to 0.01 and $T_{g,\infty}$ from 800 to 950 K, five distinct ignition regimes are identified, as summarized in Fig. 3. At the lowest temperatures in the investigated range, the system resides in a non-ignition regime. The droplet undergoes slow evaporation, and both methanol vapor and ambient hydrogen participate in weak exothermic reactions. The local heat release is too small to induce a significant temperature rise, and no thermal runaway or self-sustained flame develops within the droplet lifetime. In this regime, increasing $Y_{H_2,\infty}$ up to 0.003 does not qualitatively alter the outcome. It should be emphasized that for higher hydrogen fractions than those considered here, direct autoignition of a homogeneous hydrogen-air mixture could occur even in the absence of the droplet.

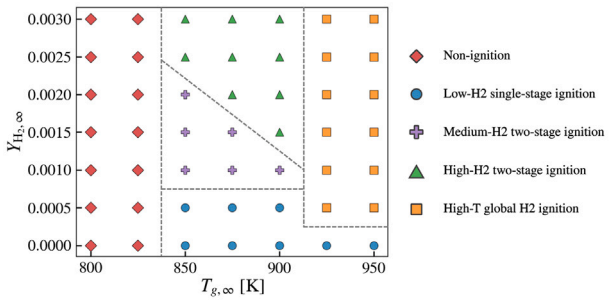

Fig. 3. Ignition regime map in the ($T_{g,\infty}$, $Y_{H_2,\infty}$) parameter space for a methanol droplet in hydrogen-enriched air. Five regimes are identified, and the boundaries are based on a finite set of computations and should be interpreted as approximate transitions rather than sharp, universal limits.

As shown in Fig. 3, for small $Y_{H_2,\infty}$, increasing the ambient temperature drives a transition into a low-hydrogen single-stage ignition regime. Here, the ignition process closely resembles that of a methanol droplet in pure air. Autoignition occurs at the outer boundary of the developing evaporating boundary layer of the methanol vapor surrounding the droplet [31], producing a single-stage ignition event. Hydrogen acts mainly as a kinetic promoter: it shortens the ignition delay by enriching the radical pool but does not fundamentally change the ignition topology or flame evolution. A representative case is illustrated in Fig. 4(a), where the radial profiles of gas temperature and OH mass fraction at several characteristic times show the formation of a localized ignition kernel that evolves into a diffusion flame surrounding the droplet.

At intermediate hydrogen levels, a qualitatively new behavior emerges: the medium-hydrogen two-stage ignition regime. In this study, ignition stages are defined based on the temporal evolution of the maximum domain temperature, $T_{g,\max}$. First-stage ignition is defined as the initial rapid rise in $T_{g,\max}$ triggered by the autoignition of the ambient hydrogen-air mixture. Second-stage ignition refers to the subsequent distinct temperature jump induced by the combustion of the methanol vapor-air mixture near the droplet. A single-stage ignition is identified when only one rapid rise in $T_{g,\max}$ occurs, while two-stage ignition is characterized by two distinct, successive temperature jumps (as illustrated in Fig. 1(c)).

A representative case at $T_{g,\infty}$ = 850 K and $Y_{H_2,\infty} = 0.001$ is shown in Fig. 4(b). The first-stage ignition occurs at a radius where the methanol-hydrogen-air mixture is prone to ignite, producing a premixed flame front characterized by sharply peaked temperature and OH profiles. The front splits into two branches: an outward-propagating flame that travels into the homogeneous hot oxidizer and an inward-propagating flame that moves toward the droplet through a region of increasing methanol concentration and stronger evaporative cooling. The outward-propagating flame gradually dies out as the ambient hydrogen-air mixture is too lean to sustain it. During this first stage, ambient hydrogen is the primary fuel consumed, with methanol contributing more significantly on the inward side of the front.

When the hydrogen enrichment is further increased, the system enters the high-hydrogen two-stage ignition regime. Fig. 4(c) illustrates a representative case at $T_{g,\infty}$ = 900 K and $Y_{H_2,\infty}$ = 0.003. The first-stage hydrogen ignition again occurs remotely and generates inward- and outward-propagating premixed flames. In this regime, however, the outward flame propagates more vigorously and can traverse the domain without appreciable attenuation, while the inward flame, after traveling through a hydrogen-rich but increasingly methanol-laden layer, triggers the second-stage ignition in the vicinity of the droplet and establishes a strongly burning diffusion flame. The spatio-temporal distributions of the mass fractions of CH_3OH, H_2, O_2, and the heat release rate in Fig. 5 clearly show the emergence of two premixed flame surfaces immediately after hydrogen ignition: the outer front moves rapidly into

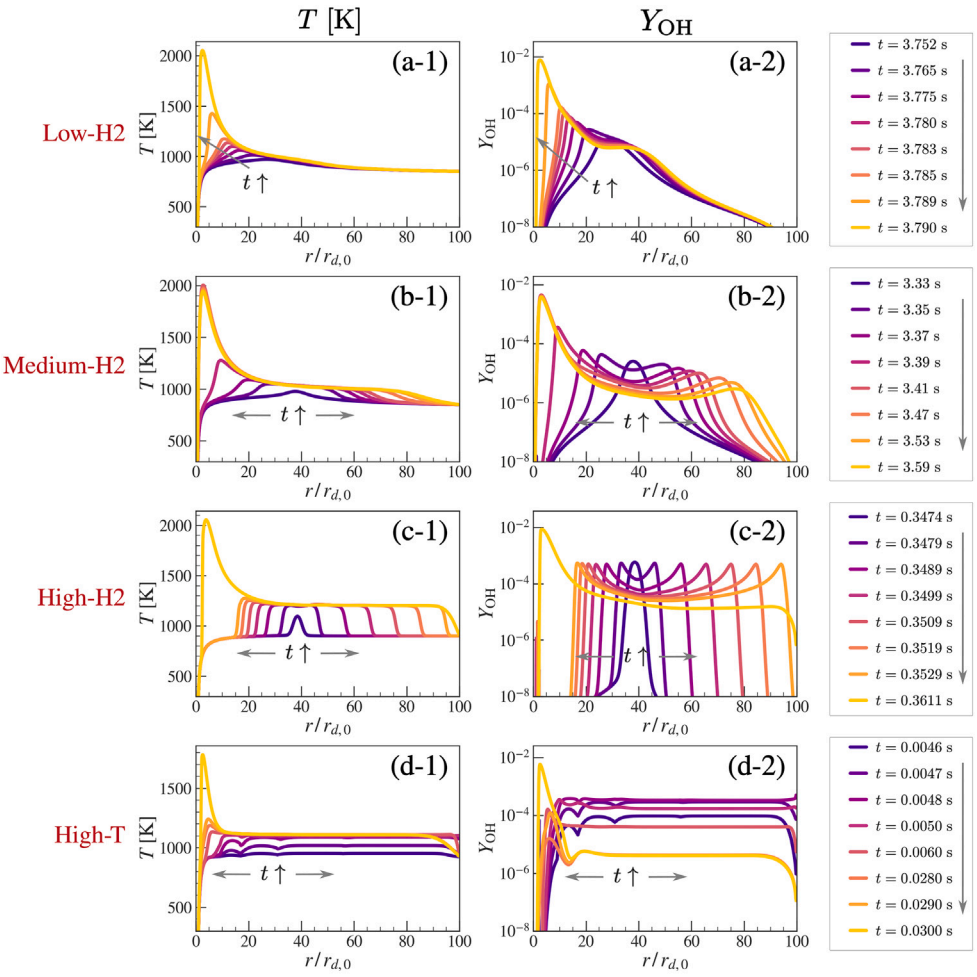

Fig. 4. Radial profiles of gas temperature (left column) and OH mass fraction (right column) at selected times for representative ignition regimes: Panel (a) shows low-hydrogen single-stage ignition at $T_{g,\infty}$ = 850 K and $Y_{H_2,\infty}$ = 0.0005; Panel (b) illustrates medium-hydrogen two-stage ignition at $T_{g,\infty}$ = 850 K and $Y_{H_2,\infty}$ = 0.001; Panel (c) presents high-hydrogen two-stage ignition at $T_{g,\infty}$ = 900 K and $Y_{H_2,\infty}$ = 0.003; and Panel (d) shows high-temperature global ignition at $T_{g,\infty}$ = 925 K and $Y_{H_2,\infty}$ = 0.002.

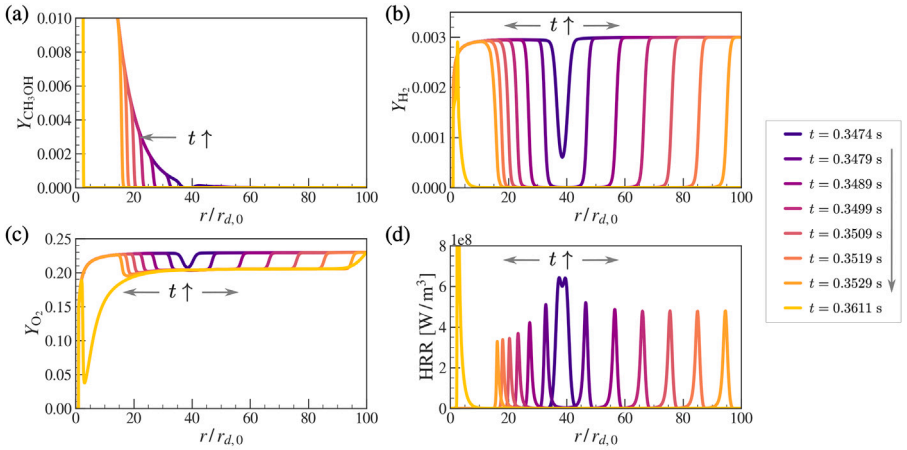

Fig. 5. Spatio-temporal evolution of key fields during the transition phase in the high-hydrogen two-stage ignition regime at $T_{g,\infty}$ = 900 K and $Y_{H_2,\infty}$ = 0.003 (corresponding to Fig. 4(c)). Shown are contours of (a) CH_3OH mass fraction, (b) H_2 mass fraction, (c) O_2 mass fraction, and (d) heat release rate (HRR).

the uniform hydrogen-air mixture, whereas the inner front slows down as it encounters strong mixture stratification and evaporative cooling. As time progresses, the inward front loses its premixed character and transforms into a diffusion flame anchored near the droplet.

At the highest temperatures examined, the system transitions into a high-temperature global hydrogen ignition regime. An example at $T_{g,\infty}$ = 925 K and $Y_{H_2,\infty}$ = 0.002 is shown in Fig. 4(d). Here, hydrogen-air chemistry is sufficiently fast such that ignition occurs

almost simultaneously over a broad radial region, producing a relatively uniform rise in temperature and OH mass fraction without a clearly identifiable localized kernel. Methanol ignition follows rapidly as the globally ignited hydrogen flame field accelerates the oxidation of methanol vapor. In this regime, hydrogen behaves effectively as a homogeneous reactive background, and the droplet primarily modulates the subsequent diffusion flame structure and burning rate rather than initiating the first-stage ignition.

The five regimes identified in Fig. 3, namely non-ignition, low-hydrogen single-stage ignition, medium-hydrogen two-stage ignition, high-hydrogen two-stage ignition, and high-temperature global hydrogen ignition, demonstrate that even modest hydrogen enrichment can fundamentally reorganize the ignition sequence and flame topology of a single methanol droplet.

3.3. Ignition delays and ignition locations

The two-stage ignition regimes are most clearly characterized by the first- and second-stage ignition delays. The first-stage delay, $t_{ig,1}$, is defined as the time from $t = 0$ to the initial rapid rise in $T_{g,\max}$ associated with remote hydrogen autoignition. The second-stage delay, $t_{ig,2}$, corresponds to the subsequent rapid temperature rise linked to the establishment of the main methanol droplet flame. In single-stage ignition cases, only $t_{ig,2}$ is defined and coincides with the classical droplet ignition delay.

According to Fig. 6, across all considered $T_{g,\infty}$, both delays decrease monotonically with hydrogen enrichment and tend toward asymptotic values at large $Y_{H_2,\infty}$. The reduction of $t_{ig,2}$ reflects the acceleration of overall chemistry due to the increased radical pool and enhanced chain-branching reactions provided by hydrogen. The emergence of a finite $t_{ig,1}$ marks the onset of the two-stage regime: once hydrogen is sufficiently abundant to ignite remotely, the first-stage delay becomes controlled primarily by hydrogen-air chemistry, and further increases in $Y_{H_2,\infty}$ yield diminishing returns.

The difference $\Delta t_{ig} = t_{ig,2} - t_{ig,1}$ provides additional insight into the coupling between hydrogen ignition and droplet ignition. For very small hydrogen enrichments, Δt_{ig} is undefined and ignition remains single-stage. As $Y_{H_2,\infty}$ enters the medium-hydrogen regime, Δt_{ig} grows, indicating that the hydrogen flame has sufficient time to develop and significantly modify the surrounding mixture before the methanol-rich near field ignites. This separation is most pronounced at intermediate $Y_{H_2,\infty}$, consistent with the well-developed two-stage structures observed in Figs. 4(b, c). At higher hydrogen levels, $t_{ig,1}$ and $t_{ig,2}$ gradually converge, signifying that the inward-propagating hydrogen flame reaches the methanol vapor layer rapidly and that the two ignition events become increasingly synchronized in time.

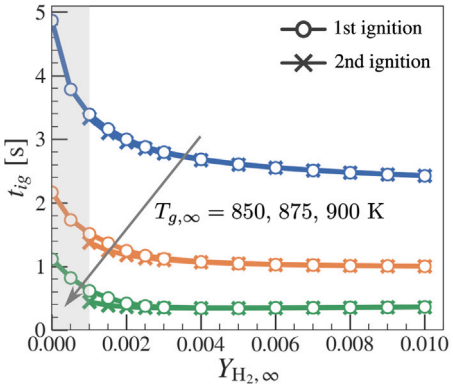

Fig. 6. First- and second-stage ignition delays as functions of ambient hydrogen mass fraction $Y_{H_2,\infty}$. The first-stage delay $t_{ig,1}$ corresponds to remote hydrogen autoignition, while the second-stage delay $t_{ig,2}$ denotes the establishment of the main methanol droplet flame. In single-stage cases, only $t_{ig,2}$ is defined.

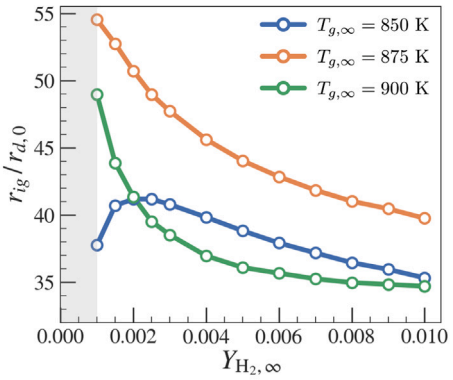

Fig. 7. Radial location of the first-stage ignition kernel as a function of ambient hydrogen mass fraction $Y_{H_2,\infty}$ at $T_{g,\infty}$ = 850, 875, and 900 K.

Beyond their temporal characteristics, the spatial locations of first-stage ignition kernels provide a complementary perspective on the influence of hydrogen. Fig. 7 presents the radial position of the first-stage ignition kernel as a function of $Y_{H_2,\infty}$ at three ambient temperatures. At $T_{g,\infty}$ = 875 and 900 K, the ignition radius decreases monotonically with hydrogen enrichment, moving progressively closer to the droplet. This behavior arises from the interplay between mixture formation and chemical reactivity. A higher initial hydrogen mass fraction reduces the distance over which methanol must diffuse to form an ignitable methanol-hydrogen-air mixture and enhances local reaction rates.

At $T_{g,\infty}$ = 850 K, the dependence becomes non-monotonic. The first-stage ignition position first increases and then decreases with $Y_{H_2,\infty}$. This non-monotonic trend reflects a delicate balance among three competing processes: evaporative cooling, diffusive enrichment of hydrogen and methanol vapor, and the strong temperature sensitivity of hydrogen and methanol oxidation. At low hydrogen levels, increased enrichment shifts the ignitable mixture farther from the droplet where evaporative cooling is weaker, leading to a larger ignition radius. At higher hydrogen levels, the enhanced chemical reactivity dominates, allowing ignition to occur closer to the droplet despite stronger evaporative cooling. Overall, the ignition-delay and ignition-location analyses demonstrate that hydrogen enrichment shortens all ignition time scales but that the spatial structure and relative timing of the two stages are strongly modulated by ambient temperature and the degree of mixture stratification.

3.4. Flame propagation dynamics

For two-stage cases, once first-stage hydrogen ignition has occurred, the resulting premixed flame fronts propagate both outward and inward through a complex, stratified dual-fuel environment. Fig. 8 illustrates the trajectories of the inward- and outward-propagating flame fronts for representative two-stage cases at $T_{g,\infty}$ = 850 and 900 K. At $T_{g,\infty}$ = 850 K, the inward flame rapidly approaches the droplet and eventually triggers the second-stage methanol ignition when it reaches the methanol-rich near field. During this interval, the outward flame propagates over a substantial radial distance. For moderate hydrogen enrichment, the outward flame speed gradually decreases as hydrogen and methanol vapor are depleted in the far field and the mixture becomes leaner. In some cases with sufficiently low ambient hydrogen, the outward flame eventually extinguishes before reaching the computational boundary.

At $T_{g,\infty}$ = 900 K, both inward and outward flames propagate more vigorously. The outward flame typically travels with nearly constant speed over a large portion of the domain and reaches $100\,r_{d,0}$ within a fraction of the interval $(t_{ig,2} - t_{ig,1})$, consistent with the propagation of a lean hydrogen-air premixed flame. This stable propagation speed arises from the nearly homogeneous thermodynamic and compositional

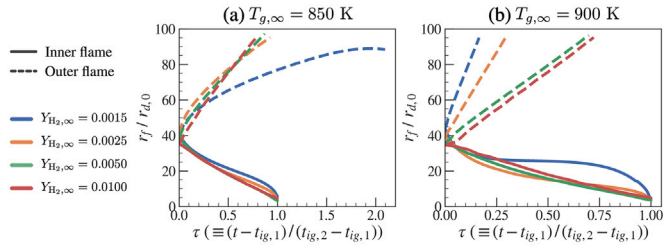

Fig. 8. Trajectories of inward- and outward-propagating flame fronts for representative two-stage ignition cases at $T_{g,\infty} = 850$ and 900 K. Flame positions are defined by the radial locations of maximum OH mass fraction. Time is normalized by $\tau = (t - t_{ig,1})/(t_{ig,2} - t_{ig,1})$, such that $\tau = 0$ and $\tau = 1$ correspond to the first- and second-stage ignition times, respectively.

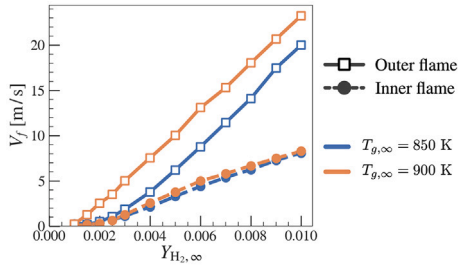

Fig. 9. Average propagation speeds of outward- and inward-propagating flames over the interval between first- and second-stage ignition, as functions of ambient hydrogen mass fraction and temperature.

conditions in the far field. In the present 1D configuration, evaporative cooling effects become negligible at sufficiently large radial distances compared to the droplet size, while the zero-gravity, quiescent setup suppresses bulk convection and hydrodynamic instabilities. As a result, the flame propagates as a spherical premixed front into a uniform mixture, yielding a generally constant flame speed. This behavior contrasts with the accelerating fronts typically observed in systems where gradients in ignition delay time are present.

The inward flame, in contrast, encounters strong gradients of temperature and composition induced by the relatively cold droplet. Depending on $Y_{H_2,\infty}$, the inward flame experiences periods of slow propagation or near-stagnation as it traverses this region. Once the inward flame reaches the stoichiometric region, the flame transitions to a stable diffusion flame anchored near the droplet.

Fig. 9 reports the average propagation speeds of inward and outward flames over the interval between the first- and second-stage ignition events. The outward flame generally propagates faster than the inward flame and, for many conditions, attains speeds comparable to the planar laminar hydrogen flame speed computed for the corresponding bulk mixture using *Cantera*. This behavior is consistent with its propagation into a nearly homogeneous hydrogen-air mixture with relatively weak thermal and compositional stratification. The inward flame, by contrast, is systematically slower, often substantially below the planar laminar value. Its propagation is strongly influenced by flame stretch, evaporative cooling, and the local consumption of both methanol and hydrogen, leading to a gradual transformation from a premixed to a diffusion-controlled flame as it approaches the droplet.

We recognize that hydrogen flames are inherently susceptible to diffusive-thermal cellular instabilities, especially under high-Reynolds-number conditions, which lie beyond the scope of a 1D spherical formulation. The 1D approximation is deliberately adopted to enable a broad parametric exploration of ambient temperature and hydrogen concentration while focusing on global ignition delays and flame front evolution. Although total flame surface area may be underpredicted, the model is believed to faithfully capture the radial gradients and kinetic timescales that control ignition onset and regime transitions.

4. Conclusions

An interface-resolved numerical study has been conducted to elucidate the autoignition and early flame dynamics of an isolated methanol droplet in hydrogen-enriched air under zero-gravity conditions. Using a VOF framework coupled with detailed gas-phase kinetics and multicomponent transport, the effects of ambient temperature and hydrogen concentration on ignition delays, ignition locations, flame topology, and flame propagation have been systematically examined. The simulations show that droplet regression approximately follows the classical d^2-law before and after ignition, and that hydrogen enrichment systematically reduces ignition delays by accelerating radical production and chain-branching chemistry, although the incremental benefit diminishes at higher hydrogen mass fractions. In contrast, the post-ignition regression rates and quasi-steady burning behavior remain only weakly affected by modest hydrogen additions.

A central outcome of this work is the identification of five ignition regimes in the $(T_{g,\infty}, Y_{H_2,\infty})$ space: non-ignition, low-hydrogen single-stage ignition, medium-hydrogen two-stage ignition, high-hydrogen two-stage ignition, and high-temperature global hydrogen ignition. Even relatively small hydrogen additions can qualitatively reconfigure the ignition sequence, shifting the first-stage ignition kernel away from the droplet, generating bi-directional flames, and at the highest temperatures producing nearly global hydrogen autoignition. The two-stage regimes arise from the strong coupling between hydrogen autoignition and methanol evaporation: an outward hydrogen flame propagates into the far field, while an inward flame traverses a stratified, methanol-rich near field and ultimately transitions into a droplet-anchored diffusion flame. Analyses of ignition delays, ignition locations, and flame propagation speeds demonstrate that hydrogen enrichment shortens all ignition time scales, but the spatial position of the first-stage ignition and the temporal separation between hydrogen and methanol ignition are highly sensitive to ambient temperature and mixture stratification.

These insights clarify the fundamental mechanisms by which hydrogen enrichment restructures dual-fuel droplet ignition and provide a physical basis for optimizing methanol-hydrogen combustion strategies in spray-based energy conversion systems. Future work should extend the present simulations to long-duration burning with water absorption, multi-dimensional effects including buoyancy, and interactions among multiple droplets in sprays.

CRediT authorship contribution statement

Zhiwu Jiang: Writing – original draft, Visualization, Validation, Methodology, Investigation, Formal analysis. **Shangpeng Li:** Writing – review & editing, Visualization, Software, Methodology. **Zheng Chen:** Writing – review & editing, Supervision. **Huangwei Zhang:** Writing – review & editing, Supervision, Project administration, Funding acquisition, Conceptualization.

Declaration of competing interest

The authors declare that they have no known competing financial interests or personal relationships that could have appeared to influence the work reported in this paper.

Acknowledgments

This work used the computational resources of the ASPIRE 1 cluster at the National Supercomputing Centre, Singapore, and the Fugaku supercomputer at the RIKEN Center for Computational Science, Japan. The authors gratefully acknowledge support from the National Research Foundation, Prime Minister's Office, Singapore, under its Campus for Research Excellence and Technological Enterprise (CREATE) program (A-0009468-00-00), the Singapore Ministry of Education Tier 2 Grant

(A-8002398-00-00), the NUS (Chongqing) Research Institute (NUSRI-CQ), and Peking University.

Data availability

Data will be made available on request.

References

[1] Khan MZA, Khan HA, Ravi SS, Turner JW, Aziz M. Potential of clean liquid fuels in decarbonizing transportation – an overlooked net- zero pathway? Renewable Sustainable Energy Rev 2023;183:113483.
[2] Olah GA, Goeppert A, Prakash GKS. Beyond oil and gas: the methanol economy. John Wiley & Sons; 2018.
[3] Verhelst S, Turner JW, Sileghem L, Vancoillie J. Methanol as a fuel for internal combustion engines. Prog Energy Combust Sci 2019;70:43–88.
[4] Azhari NJ, Erika D, Mardiana S, Ilmi T, Gunawan ML, Makertihartha IGBN, Kadja GTM. Methanol synthesis from CO_2: a mechanistic overview. Results Eng 2022;16:100711.
[5] Jadhav SG, Vaidya PD, Bhanage BM, Joshi JB. Catalytic carbon dioxide hydrogenation to methanol: a review of recent studies. Chem Eng Res Des 2014;92(11):2557–67.
[6] Zhang B, Ji C, Wang S, Zhou X. Idling performance of a hydrogen-blended methanol engine at lean conditions. Energy Procedia 2014;61:331–4.
[7] Xiao P, Wu H, Wang Z, Zhang S, Lee C-F, Wang Z, Liu F. Experimental and kinetic investigation on the effects of hydrogen additive on laminar premixed methanol–air flames. Int J Hydrogen Energy 2019;44(39):22263–81.
[8] Gong C, Li Z, Chen Y, Liu J, Liu F, Han Y. Influence of ignition timing on combustion and emissions of a spark-ignition methanol engine with added hydrogen under lean-burn conditions. Fuel 2019;235:227–38.
[9] Verhelst S. Recent progress in the use of hydrogen as a fuel for internal combustion engines. Int J Hydrogen Energy 2014;39(2):1071–85.
[10] Faeth GM. Current status of droplet and liquid combustion. Prog Energy Combust Sci 1977;3(4):191–224.
[11] Law CK. Recent advances in droplet vaporization and combustion. Prog Energy Combust Sci 1982;8(3):171–201.
[12] Sazhin SS. Droplets and sprays: simple models of complex processes, Mathematical Engineering. Springer International Publishing; 2022.
[13] Basu S, Agarwal AK, Mukhopadhyay A, Patel C. Droplets and sprays: applications for combustion and propulsion. Springer; 2017.
[14] Aggarwal SK. Single droplet ignition: theoretical analyses and experimental findings. Prog Energy Combust Sci 2014;45:79–107.
[15] Stauch R, Maas U. The ignition of methanol droplets in a laminar convective environment. Combust Flame 2008;153(1):45–57.
[16] Schnaubelt S, Moriue O, Coordes T, Eigenbrod C, Zarm HR. Detailed numerical simulations of the multistage self-ignition process of n-heptane, isolated droplets and their verification by comparison with microgravity experiments. Proc Combust Inst 2000;28(1):953–60.
[17] Takei M, Tsukamoto T, Niioka T. Ignition of blended-fuel droplet in high-temperature atmosphere. Combust Flame 1993;93(1):149–56.
[18] Cuoci A, Mehl M, Buzzi-Ferraris G, Faravelli T, Manca D, Ranzi E. Autoignition and burning rates of fuel droplets under microgravity. Combust Flame 2005;143(3):211–26.
[19] Tanabe M, Kono M, Sato J, Koenig J, Eigenbrod C, Dinkelacker F, Rath Zarm HJ. Two stage ignition of n-heptane isolated droplets. Combust Sci Technol 1995;108(1–3):103–19.
[20] Zhang W, Zhou H, Liu YC. Autoignition regime boundaries for n-heptane droplets under microgravity. Microgravity Sci Technol 2022;34(4):57.
[21] Tsai JS, Sterling AM. The combustion of linear droplet arrays. Symp Int Combust 1991;23(1):1405–11.
[22] Saufi A, Frassoldati A, Faravelli T, Cuoci A. Interface-resolved simulation of the evaporation and combustion of a fuel droplet suspended in normal gravity. Fuel 2021;287:119413.
[23] Li S, Zhang H. Simulation of single ammonia droplet combustion at elevated pressures. Combust Flame 2026;283:114534.
[24] Marchese AJ, Dryer FL, Colantonio RO, Nayagam V. Microgravity combustion of methanol and methanol/water droplets: drop tower experiments and model predictions. Symp Int Combust 1996;26(1):1209–17.
[25] Lee A, Law CK. An experimental investigation on the vaporization and combustion of methanol and ethanol droplets. Combust Sci Technol 1992;86:253–65.
[26] Kazakov A, Conley J, Dryer FL. Detailed modeling of an isolated, ethanol droplet combustion under microgravity conditions. Combust Flame 2003;134:301–14.
[27] Goodwin DG, Moffat HK, Speth RL. Cantera: an object-oriented software toolkit for chemical kinetics, thermodynamics, and transport processes. 2018.
[28] Gesellschaft VDI, Ed VDI heat atlas. Springer Berlin Heidelberg; 2010.
[29] Fernández-Tarrazo E, Sánchez-Sanz M, Sánchez AL, Williams FA. A multipurpose reduced chemical-kinetic mechanism for methanol combustion. Combust Theor Model 2016;20(4):613–31.
[30] Saufi A, Frassoldati A, Faravelli T, Cuoci A. DropletSMOKE++: a comprehensive multiphase CFD framework for the evaporation of multidimensional fuel droplets. Int J Heat Mass Transfer 2019;131:836–53.
[31] Li S, Zhang H. Theoretical insights into transient gas and liquid phase effects on the evaporation and autoignition of stationary droplets. Combust Flame 2024;268:113626.